DOI 10.5162/Ultrasonic2025/D3-a5

Non-Destructive Evaluation and Defect Characterization of Ceramic Matrix Composites Using Laser Ultrasonics

Ruben Burger[1,2], *Datong Wu*[1], *and Christian U. Grosse*[2]
[1] *Munich University of Applied Sciences HM, Lothstr. 34, 80335 München, Germany*
[2] *Technical University of Munich - Chair of Nondestructive Testing, Lichtenbergstr. 2, 85748 Garching bei München, Germany*
ruben.burger0@hm.edu, datong.wu@hm.edu

Abstract: Laser ultrasonic non-destructive testing was applied for the first time to oxide–oxide ceramic matrix composites. A fully optical setup generated and detected broadband ultrasound in both transmission and reflection modes. The measured shear wave velocity matched predictions within $5\,\%$, confirming reliable wave generation in the highly porous material. Although the current signal-to-noise ratio is modest, simple hardware upgrades could raise performance, positioning LU as a practical inline, non-contact quality-control tool for oxide–oxide CMCs.

Keywords: Ceramic Matrix Composites, Laser Ultrasonics, Non-Destructive Testing, Laser Doppler Vibrometer, Guided Waves

Introduction

Ceramic Matrix Composites (CMCs) are high-performance materials developed for use in environments demanding exceptional thermal and mechanical properties, such as those found in aerospace, energy, and defense industries [1, 2]. Unlike monolithic ceramics, which are characterized by brittleness and susceptibility to catastrophic failure, CMCs combine ceramic matrices with reinforcing fibers, resulting in enhanced toughness, damage tolerance, and resistance to thermal shocks [3].

CMCs are generally classified into Oxide-Oxide (Ox-Ox) and Non-Oxide systems. Ox-Ox CMCs typically consist of alumina (Al_2O_3) matrices reinforced with fibers such as alumina or mullite, providing excellent oxidation resistance but generally limited to lower-temperature applications compared to Non-Oxide systems [4]. In contrast, Silicon Carbide (SiC)-based CMCs, particularly SiC/SiC composites, exhibit superior high-temperature mechanical properties albeit with reduced oxidation resistance requiring protective coatings for certain applications [5].

However, the complex microstructure, inherent porosity, and anisotropic properties of CMCs create significant challenges for non-destructive evaluation (NDE). Various NDE techniques have been investigated for evaluating CMCs, each with distinct advantages and limitations. X-ray Computed Tomography (CT) offers high-resolution imaging and deep penetration capabilities, ideal for detecting internal porosity and cracks, but it is limited by high costs, long scan times, and requirements for specialized facilities [6].

Active Infrared Thermography (IRT) has demonstrated rapid, large-area inspection capabilities and effective detection of subsurface defects through thermal contrast, particularly beneficial for monitoring damage progression in CMCs under mechanical stress [7]. However, IRT's utility is limited by shallow penetration depth, sensitivity to surface emissivity variations, and thermal diffusion-induced image blurring, complicating accurate defect characterization.

Terahertz Time-Domain Spectroscopy (THz-TDS) has emerged as another non-destructive method, capable of detecting internal porosity, delaminations, and moisture ingress, with the advantage of higher resolution than microwaves and better penetration than IR techniques. The technique was applied by the authors to Ox-Ox CMC successfully [8]. Nonetheless, its widespread application is limited by significant signal attenuation in ceramics, slow data acquisition rates, and the high cost of equipment [9].

Conventional pulse-echo or immersion contact based ultrasonic testing remains the industrial baseline for CMC inspection [6]. It can detect delaminations and bulk porosity when adequate acoustic coupling is achieved. However, the open porosity and rough surfaces typical of Ox-Ox CMCs cause strong scattering and attenuation of high-frequency waves; furthermore, liquid couplants can infiltrate the pore network, complicating processing.

Air-coupled ultrasound (ACU) avoids the problems with liquid couplants by using impedance-matched membrane or capacitive transducers to transmit and receive sound through air. Vasechko et al. [10] demonstrated through-transmission ACU C-scans on porous alumina-fibre CMCs up to $16\,\mathrm{mm}$ thick, accurately mapping delaminations and high-porosity regions in agreement with CT data. Owing to the large

DOI 10.5162/Ultrasonic2025/D3-a5

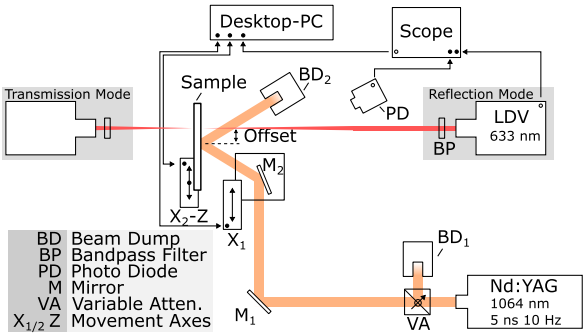

Fig. 1: Laser ultrasonic measurement setup. Sample can be moved in horizontally and vertically and the distance between excitation and measurement spots horizontally. Both transmission and reflection mode is possible with repositioning of the LDV. See details in text.

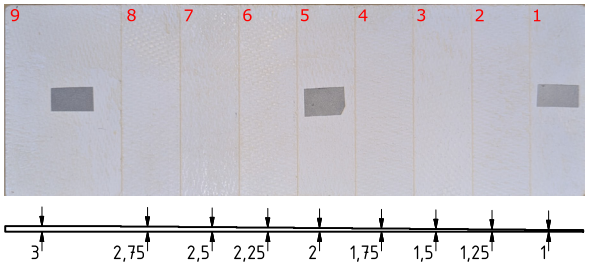

Fig. 2: Top: photograph of the front surface with three strips of reflective tape that serve as LDV targets in transmission. Red numerals label the individual steps and are used as identifiers in the text. Bottom: schematic of the stepped thickness profile.

air-to-ceramic impedance mismatch, ACU is most effective in transmission mode and typically employs narrow-band signals below $300\,\mathrm{kHz}$ which lengthens scan times.

Laser ultrasonics (LU) is a fully non-contact NDE technique in which a short-pulse laser excites broadband ultrasonic waves, while surface displacements are monitored remotely with a laser interferometer [11]. Quintero et al. [12] demonstrated that LU in through transmission geometry can visualize impact damage and delaminations in turbine-grade SiC/SiC (non-oxide) panels with image quality comparable to immersion C-scans. Ox-Ox CMCs exhibit markedly higher open porosity and acoustic attenuation due to scattering, factors that complicate wave propagation and have so far precluded LU studies.

To the authors' knowledge, the work reported here is the first systematic investigation of LU inspection for oxide–oxide CMCs, evaluating its feasibility in both through-transmission and single-surface reflection geometries.

Methods

The fully optical laser–ultrasonic setup illustrated in Figure 1 and provides a standoff distance of over $50\,\mathrm{cm}$ for both ultrasonic generation and detection. Broadband ultrasonic waves are generated by photoelastic excitation using a Q–switched Nd:YAG laser (InnoLas Spitlight 200, $1064\,\mathrm{nm}$ wavelength, $5\,\mathrm{ns}$ pulse width, $10\,\mathrm{Hz}$ repetition rate). The pulse energy, adjusted with a variable attenuator (VA), is fixed at $50\,\mathrm{mJ}$. The unfocused beam is routed to the CMC-sample via mirrors ($\mathrm{M}_{1/2}$), producing a Gaussian spot with a $5\,\mathrm{mm}$ $1/e^2$ diameter on the sample surface. The resulting fluence of $130\,\mathrm{mJ\,cm^{-2}}$ is well below the damage threshold of the Ox-Ox CMC.

The excitation spot can be translated over $50\,\mathrm{mm}$ along the x-axis (stage X_1) using a motorized linear stage. An angle of incidence of $45°$ leaves the normal direction unobstructed for detection; the reflected pump beam is absorbed by a beam dump (BD2).

The sample is mounted on a custom 3D printed mount that offers travel of $50\,\mathrm{mm}$ in both horizontal and vertical directions.

Surface vibration is monitored with a heterodyne laser Doppler vibrometer (Polytec OFV-505, $633\,\mathrm{nm}$ wavelength, $25\,\mathrm{MHz}$ $3\,\mathrm{dB}$ bandwidth, $1\,\mathrm{mW}$ output power). A $5\,\mathrm{nm}$ bandpass filter centered at $633\,\mathrm{nm}$ suppresses optical crosstalk from the pump laser. The analog LDV signal is digitized at $2.5\,\mathrm{GS\,s^{-1}}$ with a Rohde&Schwarz RTA4000 oscilloscope, triggered by a fast photodiode that monitors the pump pulse.

Stage motion, trigger synchronization, LDV autofocus, and data acquisition are controlled by a custom `.NET` application. By repositioning the LDV head, the setup supports both reflection and transmission geometries without altering the pump-beam optics (cf. Fig.1).

The $\mathrm{Al_2O_3}$ Ox-Ox CMC sample (cf. Fig.1) investigated in this work is a $300\,\mathrm{mm}$ by $100\,\mathrm{mm}$ step wedge with variation in thickness ($1\,\mathrm{mm}$ to $3\,\mathrm{mm}$ with steps of $0.25\,\mathrm{mm}$). The steps are numbered sequentially with increasing thickness. It was previously investigated using THz-TDS in reflection mode [8]. Artificial damage was not introduced. The surface is not coated or modified to increase excitation laser absorption and is also not smoothed to improve LDV signal. At $\approx 30\,\%$ porosity, the material exhibits strong attenuation for elastic waves in the MHz range. The elastic modulus of the material normal to the fiber orientation is considerably lower, leading to low wave velocities in the range of $2600\,\mathrm{m\,s^{-1}}$ ($1500\,\mathrm{m\,s^{-1}}$) for the longitudinal (shear) mode. In the photoelastic range, the excitation is dominated by the shear mode. The excited area is large relative to the thickness

DOI 10.5162/Ultrasonic2025/D3-a5

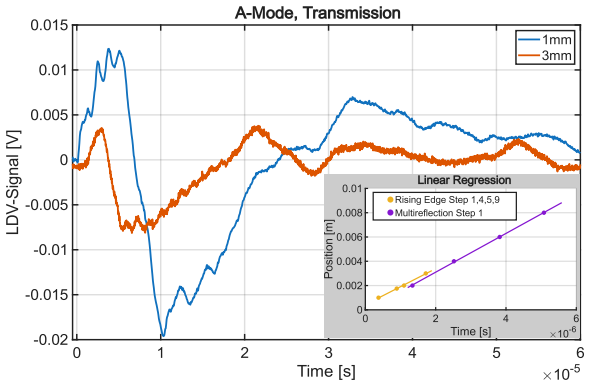

Fig. 3: A-mode signal of the thickest and the thinnest part of the sample. First peaks correspond to the arrival of the shear mode. For the thinnest areas, multiple reflections of the shear mode can be observed. Inset show linear regression for the arrival times using two method (c.f. main text).

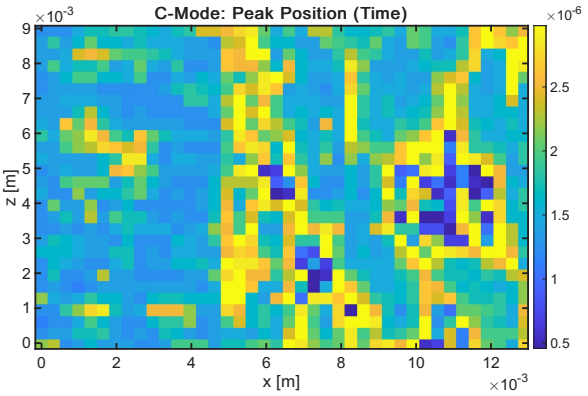

Fig. 4: C-mode image of transmission measurement across step 8 to 9. The colormap corresponds to the position in time of the first positive peak. The step is located at around $x = 5\,\mathrm{mm}$. The pattern corresponds to the varying coupling of the reflective tape due to changing surface quality between steps.

to reduce beam directivity [11, 12]. In transmission mode, reflective tape was applied to the measurement spots to increase the signal-to-noise ratio (SNR) and protect the LDV from partial transmission of the excitation pulse through the sample. This is especially important for the thinner section, where even the LDV laser shines through the sample. With reflective tape, the signal was averaged 10 times for all positions. The excitation and measurement spots were aligned for central overlap using the X_1-stage. C-Scan data was collected on a 30 by 40 grid (steps: $0.33\,\mathrm{mm}$) by moving both sample stages (X_2,Z). In reflection mode, linear scans with increasing distance between excitation and measurement were performed to track guided wave propagation, starting from direct overlap (allowing for impulse echo measurements) to a distance of $2\,\mathrm{mm}$ in steps of $0.25\,\mathrm{mm}$. Since no reflective tape was used in this measurement mode, the number of averages was set to 50 to compensate for the high measurement noise. Due to the long measurement times, no C-Scans were performed in this mode. For both measurements, at each position the LDV was refocused by the measurement application to achieve better signal quality on the rough surface of the sample.

Results and Discussion

The results of the transmission measurements are shown in Figs. 3 and 4. The received signal has a bandwidth of approximately $1\,\mathrm{MHz}$, considerably lower than the $5\,\mathrm{ns}$ excitation pulse would generates. The signals in Figure 3 are the average of a 3 by 3 pixel area with good coupling between the sample and the reflective tape. To validate the origin of the first peaks, two methods are used: tracking the rising edge of the signal across four thicknesses and tracking multiple reflections of the pulse for the thinnest step. Both regression results are shown in the inset of Figure 3. The calculated velocity is $v = 1484(220)\,\mathrm{m\,s^{-1}}$ and $v = 1587(98)\,\mathrm{m\,s^{-1}}$, respectively, confirming the origin of the signal as the shear mode. Longitudinal mode signals could not be detected in any of the measurements. The observed voltage amplitudes correspond to surface displacements of around $0.5\,\mathrm{nm}$. The C-mode image in Figure 4 shows the peak position in time of the first positive peak between steps 8 and 9. The edge is located around $x = 5\,\mathrm{mm}$ and can be clearly identified in the data. The observed pattern corresponds to the surface quality of the scan area: On the left, the surface is smooth and thus shows good coupling to the reflective tape. On the right, the ceramic fibers are bare, leading to very uneven coupling.

An example of the reflection mode measurements is shown in Figure 5. The characteristic dispersive A_0 Lamb mode can be clearly identified for the full scan range. Further modes could not be detected due to low SNR. The inset of Figure 5 shows the impulse-echo signal at overlap between excitation and detection. The peak position is in agreement with the shear velocities observed in transmission mode.

This study confirms that LU NDT is a promising tool for Ox-Ox CMC inspection. The measured wave speeds align with the expected shear-wave velocity of the composite, validating both the optical generation scheme and the material model. Reflection-mode data show clear elastic arrivals, indicating that LU can be adapted for in-service inspections where only a single surface is accessible.

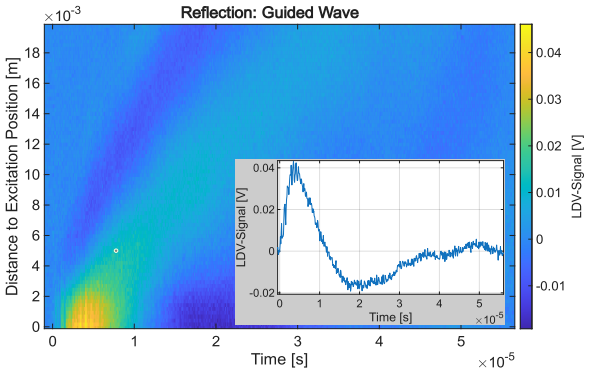

Fig. 5: Linear Scan in reflection mode (time vs. excitation distance) at step 7. Dispersive guided wave mode (A0 Lamb) is clearly visible. Inset shows impulse echo signal at overlap.

Although the current signal-to-noise ratio is modest, several straightforward upgrades are available:

1. *Excitation.* Switching to ultraviolet pulses with slightly longer durations could increase surface absorption and preferentially excite the sub-$1\,\mathrm{MHz}$ bandwidth that propagates efficiently in porous media.

2. *Detection.* Modern LDVs featuring active speckle tracking will better accommodate surface roughness and deliver higher amplitude fidelity.

3. *Scanning speed.* Replacing mechanical stages with galvanometric or MEMS mirrors will cut acquisition time by an order of magnitude.

Future work should focus on these hardware improvements and extend the study to production-grade components with complex geometries. Collectively, these efforts will advance LU-NDT toward a robust, shop-floor-ready technology for the quality assurance of Ox-Ox CMC structures.

References

[1] R. Naslain. "Design, preparation and properties of non-oxide CMCs for application in engines and nuclear reactors: an overview". In: *Composites Science and Technology* 64.2 (2004), pp. 155–170.

[2] W. Krenkel. *Ceramic matrix composites: fiber reinforced ceramics and their applications*. John Wiley & Sons, 2008.

[3] A. Evans and D. Marshall. "Overview no. 85 The mechanical behavior of ceramic matrix composites". In: *Acta Metallurgica* 37.10 (1989), pp. 2567–2583. DOI: 10.1016/0001-6160(89)90291-5.

[4] C. G. Levi et al. "Processing and performance of an all-oxide ceramic composite". In: *Journal of the American Ceramic Society* 81.8 (1998), pp. 2077–2086.

[5] R. Naslain et al. "Oxidation mechanisms and kinetics of SiC-matrix composites and their constituents". In: *Journal of materials science* 39 (2004), pp. 7303–7316.

[6] N. Ida and N. Meyendorf. *Handbook of advanced nondestructive evaluation*. Vol. 10. Springer International Publishing Cham, Switzerland, 2019.

[7] K. G. Dassios et al. "Nondestructive Damage Evaluation in Ceramic Matrix Composites for Aerospace Applications". In: *The Scientific World Journal* 2013.1 (2013), p. 715945. DOI: 10.1155/2013/715945.

[8] D. Wu et al. "Application of terahertz time domain spectroscopy for NDT of oxide-oxide ceramic matrix composites". In: *Infrared Physics & Technology* 102 (2019), p. 102995. DOI: 10.1016/j.infrared.2019.102995.

[9] F. Ellrich et al. "Terahertz quality inspection for automotive and aviation industries". In: *Journal of Infrared, Millimeter, and Terahertz Waves* 41 (2020), pp. 470–489.

[10] V. Vasechko et al. "Air-coupled ultrasonic inspection technique as NDT tool for evaluation of porous wound oxide/oxide composite ceramics". In: *Proceedings of the 19th World Conference of Non-Destructive Testing, Munich, Germany*. 2016, pp. 13–17.

[11] C. Scruby and L. Drain. *Laser Ultrasonics Techniques and Applications*. CRC Press, 1990.

[12] R. Quintero et al. "Noncontact laser ultrasonic inspection of Ceramic Matrix Composites (CMCs)". In: *NDT & E International* 88 (2017), pp. 8–16. DOI: 10.1016/j.ndteint.2017.02.008.